Multimode power processing interface for fuel cell range extender in battery powered vehicle

Article *in* Applied Energy · October 2017

DOI: 10.1016/j.apenergy.2017.07.043

3 authors:

Ilan Aharon
Tel Aviv University
15 PUBLICATIONS **460** CITATIONS
SEE PROFILE

Doron Shmilovitz
Tel Aviv University
148 PUBLICATIONS **1,441** CITATIONS
SEE PROFILE

Alon Kuperman
Ben-Gurion University of the Negev
129 PUBLICATIONS **1,133** CITATIONS
SEE PROFILE

Multimode Power Processing Interface for Fuel Cell Range Extender in Battery Powered Vehicle

Ilan Aharon[1,3], Doron Shmilovitz[1]and Alon Kuperman[*2,3]

[1]School of Electrical Engineering
Dept. of Physical Electronics, Tel Aviv University
POB 39040, Tel Aviv 69978, Israel

[2]Applied Energy Center
Dept. of Electrical and Computer Engineering, Ben-Gurion University
POB 653, Beer-Sheva84105, Israel

[3]Hybrid Energy Sources Laboratory
Dept. of Electrical Engineering and Electronics, Ariel University
POB 3, Ariel 40700, Israel

[*]Corresponding Author, Tel: +972-526943234, Email: alonk@bgu.ac.il.

ABSTRACT

Uninhabited electric vehicle typically utilize batteries as an exclusive power source. In order to remedy the limited energy density and thus operation time of the battery-powered unmanned vehicles, fuel based range extenders are often utilized. The operation strategy for the range extender is to maximize the mission endurance therefore it should operate at minimum specific fuel consumption point. Furthermore, the source and load voltage level may differ, hence non-inverting Buck-Boost converter (NBC) is conjoint them while keeping the desire operation point. This paper proposes a fuel cell (FC) based range extender, interfaced to the main power bus by cascade output power regulation strategy for NBC. The NBC is based on unique modulator that produces switching sequence for both converter legs. The modulator receive single control input from the dual loop regulator, inner inductor current loop and outer output power loop, which is common for energy management strategies of hybrid energy sources. System design commences with regulator design based on small signal analysis of NBC, and then it is shown that the suggested control architecture allows tight output power control throughout the entire operating range despite various plants. Finally a case study is presented, in which the converter operates as power processing interface of a fuel cell, operating as range extender in an all-electrical aircraft. The revealed findings are well-supported by simulation and experimental results.

Keywords: Non-inverting buck-boost converter, power control, fuel cell, range extender.

NOMENCLATURE

NBC	Non-inverting Buck-Boost Converter
FC	Fuel Cell
ICE	Internal Combustion Engine
Li-Po	Lithium Polymer
UA	Uninhabited Aircraft
PEM	Proton Exchange Membrane
MEP	Maximum Efficiency Point
MSFC	Minimum Specific Fuel Consumption
MPP	Maximum Power Point
PWM	Pulse Width Modulation
BW	Bandwidth
v_{BUS}	Bus Voltage
PI	Proportional Integral
p_L	Load Power
v_S	Input Source Voltage
i_L	Inductor Current
i_{REF}	Reference Current
v_O	Output Source Voltage
p_O	Output Power
p_{REF}	Reference Power

I. INTRODUCTION

The concept of range extension involves utilizing high-energy sources to enhance vehicle endurance. High theoretical efficiency, zero emissions operation and low thermal and acoustic signatures of FC make them one of the most promising candidates to replace the internal combustion engine (ICE) as the high-energy source in electric vehicle applications. Nevertheless, since the dynamic response of FCs is restricted, hybridizing with a dynamic source is essential [1], [2]. In general, instantaneous load power P_L can be decomposed into two components: steady (average) power $P_{l,avg}$ and zero average dynamic power $P_{l,dyn}$. A typical uninhabited aircraft (UA) contains a single energy source (ICE or battery pack), supplying both components of P_L. When quiet and/or emission-free operation is required, electrical propulsion is preferred. Unfortunately, limited energy density of modern batteries restricts operation time of the UA. Moreover, since typical UA mission requires high take-off power, high-energy batteries cannot be used because of the power-energy trade-off. As a solution, splitting the electrical source into an energy unit (FC) and power unit (battery) is proposed in this paper, creating a DC micro-grid shown in Fig. 1. There, the FC is responsible for steady-state operation (cruising) and hence ideally supplies the average power $P_{l,avg}$ (determining the mission length), while the battery is answerable for the transient-state operation (take-off and maneuvering) and therefore supplies the dynamic power $P_{l,dyn}$. Consequently, the range extender is expected to inject a power with slow dynamics into the system in order to enhance the operating range of the UA. Theoretically, this leaves the battery to supply the dynamic component of the load power only.

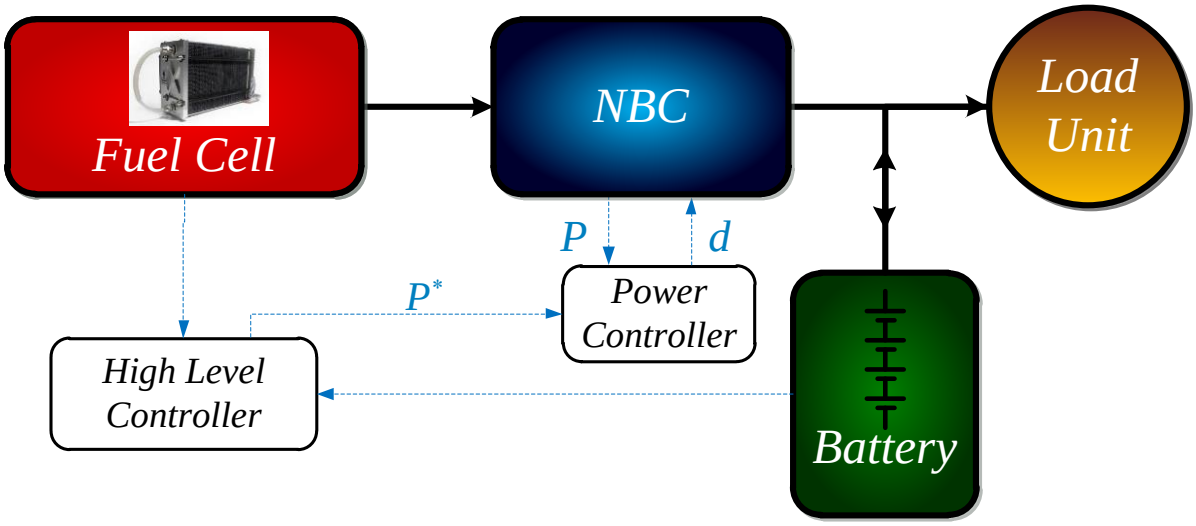

Fig. 1. Case study topology. P^* and P denote reference and actual NBC output power, d symbolizes control input to the converter.

The progress of the FC technology has recently resulted in releasing a series of commercial devices to the market. Proton Exchange Membrane (PEM) based FC (converting hydrogen to electricity) is probably the most common off the shelf technology. Several companies produce PEM FC stacks at 30W – 5000W power ratings [3]. A significant barrier for PEM FC widespread use is the use of hydrogen, which is extremely flammable. Another disadvantage is the fact that when stored in a typical high-pressure cylinder (~200 bar), hydrogen represents only 6% of the total weight. One of the solutions for both mentioned problems is a hydrogen generator, which blends borohydride with water to produce hydrogen [4]. The Aeropak by Horizon Fuel Cell Technology is one of the off-the-shelf products, utilizing this method. The unit is capable of supplying up to 200 W continuously, achieving the energy density of circa 700 Wh/kg.

It is well known, that FC possesses an optimal operating point, referred to as “Maximum Efficiency Point” (MEP) or the “Minimum Specific Fuel Consumption” (MSFC), where the specific fuel consumption (amount of fuel consumed for producing a unit of electrical

energy) is minimal [1]. It should be mentioned that the FC power output at MEP is lower than the device rated power, referred to as "Maximum Power Point" (MPP). In addition, the FC is a soft source [5], possessing nonlinear static I-V characteristics and may be defined either as voltage, current or power source.

Switching power converters are the most common energy processing units for power delivery in modern renewable and alternative energy related applications. Micro-grid is one of the most evolving discipline, formed by distributed energy resources with clearly defined electrical boundaries acting as a single controllable entity with respect to the main grid and can be connected to and disconnect from the grid to enable both grid-connected or island mode operation [6],[7]. In DC micro-grids sources, storage and loads are connected by power converters to one or more common DC buses [1]. Three basic conversion topologies (buck, boost and buck boost) are typically achieved by utilizing three basic dedicated circuitries while basic buck-boost converter suffers from relatively low efficiency and polarity inversion. As a remedy, NBC is capable of stepping the output voltage up and down, based on cascaded connection of basic buck and boost stages sharing a common inductor was proposed in [8]-[10]. The NBC was used in applications such as power factor correction [11], maximum power point tracking in photovoltaic cells [12]-[13], fuel cell voltage regulation[14]-[17],battery charging [10], [15],[18], electrical vehicle [19]-[23]and micro-grids [24]-[25]. In all the mentioned applications, DC/DC converter was used to obtain regulated either input or output voltage [26].

During NBC operation, multiple mode transitions occur, resulting in time-varying nonlinear behavior which increases the control challenge. The controller is required to drive both buck and boost legs with different pulse width modulation (PWM) sequences [27]. One of the main drawbacks of proposed methods is the non-smoothness of mode transitions, requiring careful treatment. Recently, a modulator receiving a single control signal from the

inner current loop controller and driving both converter legs was proposed in [27]. The NBC with the proposed circuitry was shown to automatically benefit from smooth mode transitions. The feature is particularly important when interfacing a low-dynamics energy source such as fuel cell.

In order to both enhance disturbance rejection and obtain tight current regulation, dual-loop control structures were proposed in [27]-[30] for NBCs with classical modulators. Inner loop current control for the NBC with the improved modulator was discussed in [27]. It was shown that the small signal representation of the converter is different from the classical one due to the non-similar modulator.

As mentioned above, in most of NBC applications, input or output voltage is the controlled variable. Nevertheless, when operating as power processing interface of a unidirectional energy source, power control rather than voltage control is required in case DC bus voltage forming is carried out by another unit/s. Energy management algorithm is usually executed by a high-level controller, which generates power reference command/s to all the controlled source/storage units. Therefore, small-signal system analysis of the power conversion interface is required with output power playing the role of output loop controlled variable, taking into account the behavior of units, connected to its input and output terminals.

In this paper, NBC with the improved dual carrier modulator operating in a typical DC micro-grid is analyzed and operated by cascaded control structure to regulate output power. Simple dual loop controller is designed and system performance is analyzed for the whole expected operating range. As a case study, the proposed circuitry operates as power processing interface of a FC, operating as a range extender for a battery powered aerial vehicle. The NBC topology is selected since while Li-Po battery terminal voltage varies as a function of the state of charge, output voltage of the fuel cell undergoes significant changes

according to operating power. System stability and robustness analysis is also given in order to verify the correct operation at different operational extremes. Experimental prototype is built and tested to verify the feasibility of the proposed analysis.

II. SYSTEM MODELING

The NBC under study is depicted in Fig. 2.The power stage is formed by cascaded connection of two synchronous converter legs, sharing a common inductor *L*. High-frequency bypass capacitors C_{in} and C_{out} are intended to suppress switching frequency ripples at the converter terminals. Both legs are driven by different PWM signals with corresponding duty cyclesd_1 and d_2, where $d_{1,2} \in [0,1]$ denote the duty ratios for buck and boost legs respectively, derived from the modulator control input $d \in [-1,1]$. In Fig. 2, $v_S(t)$, $i_L(t)$ and $v_O(t)$ represent the converter input voltage, inductor current and output voltage, respectively. Note that the duty ratio $d_1 \in [0,1]$ causes the switch $Q_1(\bar{Q}_1)$ to be turned on (off) for a period $d_1 T$ and to be turned off (on) for a period $(1-d_1)T$. Likewise, the duty ratio $d_2 \in [0,1]$ causes the switch $Q_2(\bar{Q}_2)$ to be turned on for a period $d_2 T$ and to be turned off (on) for a period $(1-d_2)T$, where T denotes PWM switching period.

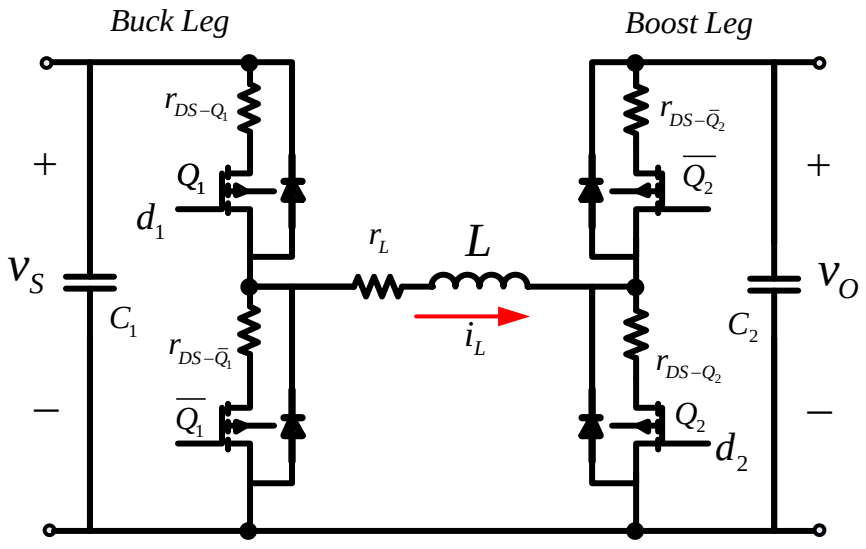

Fig. 2. Synchronous non-inverting buck-boost converter.

The operation of each leg is derived from the behavior of appropriate basic converter. In case $v_S > v_O$ the NBC is set to operate in buck mode, i.e. switches of leg 1 are driven by a PWM signal while Q_2 is off and $\bar{Q}_2$ is on. In contrary, if $v_S < v_O$ the NBC is set to operate in boost mode, i.e. the switches of leg 2 are driven by a PWM signal while Q_1 is on and $\bar{Q}_1$ is off. Finally, if $v_S \approx v_O$ (the limits will be discussed later on), both legs are PWM driven and the converter operates in buck-boost mode.

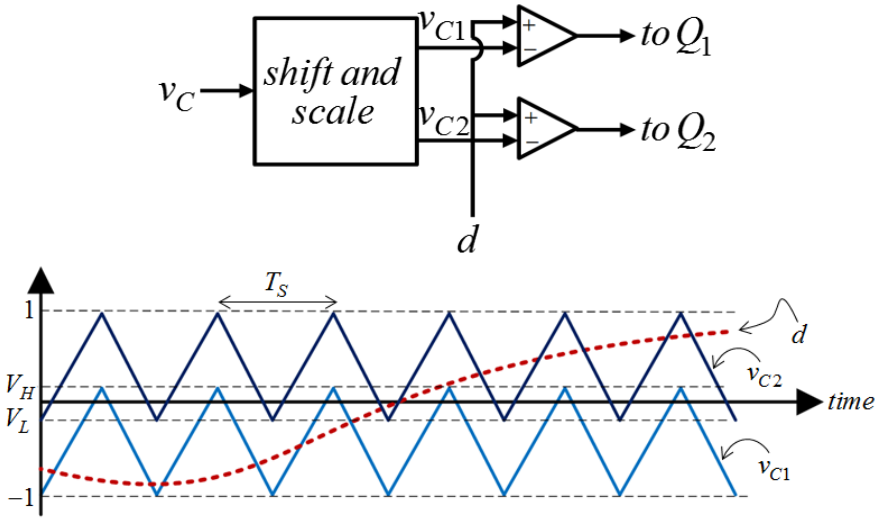

Fig. 3. Modulator structure (top) and corresponding waveforms (bottom).

In order to achieve the mentioned functionality and smooth transition between the operation modes, the modulator proposed in [27] is utilized, as shown in Fig. 3.The triangular carrier v_C is scaled and then duplicated using different shift factors to create buck and boost legs carriers. The control signal -1 <d< 1 is then compared to both carriers in order to create PWM driving signals for each leg. The corresponding duty cycles of buck and boost legs are then given by

$$d_1 = \begin{cases} 0, & d \le -1 \\ K_H(1+d), & -1 \le d \le V_H \\ 1, & d \ge V_H \end{cases} \quad (1)$$

and

$$d_2 = \begin{cases} 0, & d \le V_L \\ K_L(d - V_L), & V_L \le d \le 1 \\ 1, & d \ge 1 \end{cases}, \tag{2}$$

respectively, with $K_H = (1 + V_H)^{-1}$ and $K_L = (1 - V_L)^{-1}$. Converter static voltage transfer function and operating mode are then dictated solely by control input as

$$M(D) = \frac{V_O}{V_S} = \begin{cases} K_H(1+D), & buck \\ \dfrac{K_H(1+D)}{K_L(1-D)}, & buck-boost \\ \dfrac{1}{K_L(1-D)}, & boost \end{cases}, \tag{3}$$

and

$$Operating\ Mode = \begin{cases} buck, & -1 < d < V_L \ or\ M(D) < \dfrac{1+V_L}{1+V_H} \\ buck-boost, & V_L < d < V_H \ or\ \dfrac{1+V_L}{1+V_H} < M(D) < \dfrac{1-V_L}{1-V_H} \\ boost, & V_H < d < 1 \ or\ M(D) > \dfrac{1-V_L}{1-V_H}. \end{cases} \tag{4}$$

where D, V_S and V_O are the steady-state (DC) components of d, v_S and v_O, respectively.

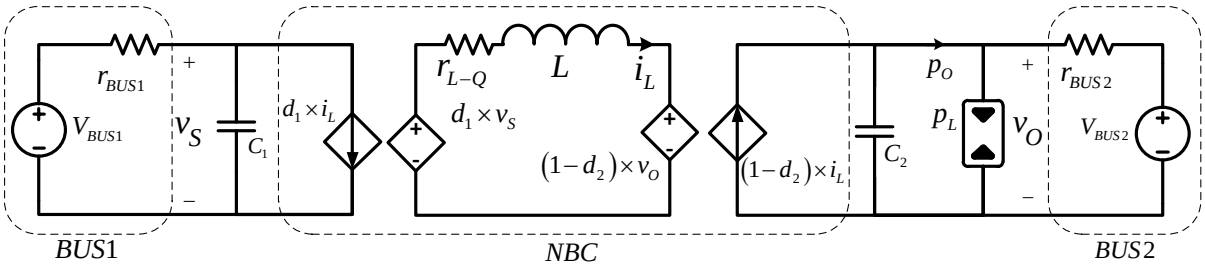

Fig. 4. Average model of the system.

The average model of the system is presented in Fig. 4 (for additional details on deriving the average NBC model, an interested reader is referred to [27]). Moreover, a lumped

parasitic resistance of the inductor and the two conducting MOSFETs is marked as r_{L-Q}. It is assumed that input port of the converter (BUS1) is connected to an energy source represented by its Thevenin equivalent (V_{BUS1}, r_{BUS1}) while its output port (BUS2) is connected to a micro-grid, represented by a Thevenin equivalent (V_{BUS2}, r_{BUS2}) in parallel with constant power element p_L [25].

From Fig. 4, average system dynamics is highly nonlinear, given by

$$\begin{aligned} C_1 \frac{dv_S}{dt} &= \frac{V_{BUS1} - v_S}{r_{BUS1}} - d_1 i_L \\ L \frac{di_L}{dt} &= d_1 v_S - (1-d_2) v_O - i_L r_{L-Q} \\ C_2 \frac{dv_O}{dt} &= (1-d_2) i_L + \frac{V_{BUS2} - v_O}{r_{BUS2}} - \frac{p_L}{v_O}. \end{aligned} \tag{5a}$$

The NBC output power may then be obtained as

$$p_O = p_L + p_{BUS2} = p_L - \frac{V_{BUS2} - v_O}{r_{BUS2}} v_O \tag{5b}$$

Combining (5) with (1) and (2), system dynamics in each of the operation modes may be expressed as a function of the control input d as

$$\begin{aligned} C_1 \frac{dv_S}{dt} &= \frac{V_{BUS1} - v_S}{r_{BUS1}} - K_H (1+d) i_L \\ L \frac{di_L}{dt} &= K_H (1+d) v_S - v_O - i_L r_{L-Q} \\ C_2 \frac{dv_O}{dt} &= i_L + \frac{V_{BUS2} - v_O}{r_{BUS2}} - \frac{p_L}{v_O} \end{aligned} \tag{6a}$$

in buck mode,

$$\begin{aligned} C_1 \frac{dv_S}{dt} &= \frac{V_{BUS1} - v_S}{r_{BUS1}} - K_H (1+d) i_L \\ L \frac{di_L}{dt} &= K_H (1+d) v_S - K_L (1-d) v_O - i_L r_{L-Q} \\ C_2 \frac{dv_O}{dt} &= K_L (1-d) i_L + \frac{V_{BUS2} - v_O}{r_{BUS2}} - \frac{p_L}{v_O} \end{aligned} \tag{6b}$$

in buck-boost mode and

$$
\begin{aligned}
C_1 \frac{dv_S}{dt} &= \frac{V_{BUS1} - v_S}{r_{BUS1}} - i_L \\
L \frac{di_L}{dt} &= v_S - K_L(1-d)v_O - i_L r_{L-Q} \\
C_2 \frac{dv_O}{dt} &= K_L(1-d)i_L + \frac{V_{BUS2} - v_O}{r_{BUS2}} - \frac{p_L}{v_O}
\end{aligned}
\tag{6c}
$$

in boost mode. Apparently, the dynamics is different in each operation mode.

III. CONTROL DESIGN

Typical cascaded control structure of a NBC is shown in Fig. 5a [27]. Usually, one of the terminal variables is chosen to be stabilized, i.e. y may denote input or output voltage/current/power and y_{REF} is the corresponding reference signal, while inner loop controller forces an intermediate variable x to follow outer controller generated reference x_{REF}. Here, the converter output power p_O is chosen as the control variable, as depicted in Fig. 5b. The outer loop controller (which is actually a power controller here) generates a current reference signal i_{REF}, which in the case of average current control (adopted here) corresponds to inductor current i_L, averaged over one switching cycle. The current error is processed by the inner loop controller and generates the control input d to the PWM module [27], [30], [31].

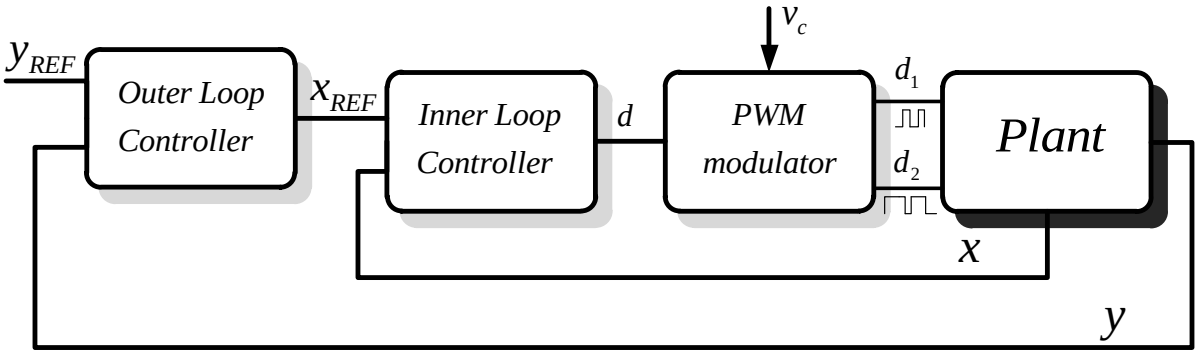

(a)

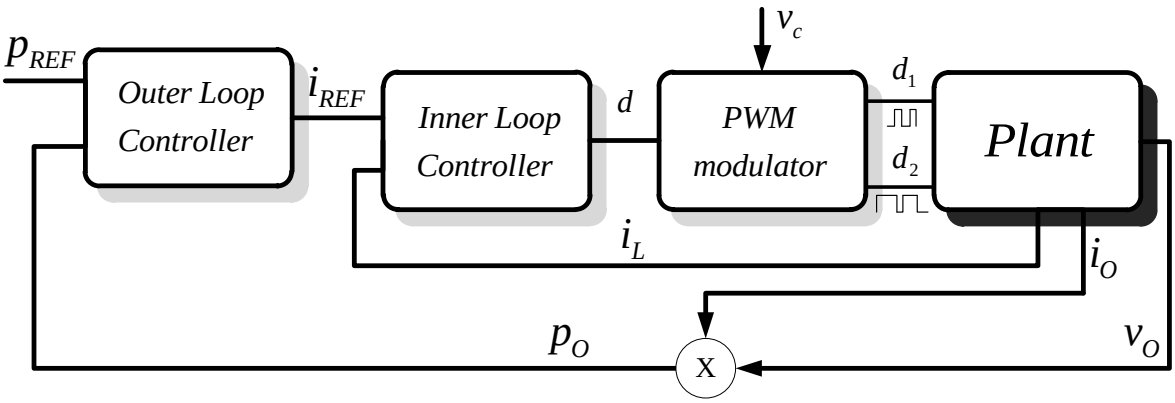

(b)

Fig. 5. Cascaded control structure of a NBC. (a) Generalized, (b) Adopted in the study.

The two loops are decoupled in frequency domain to allow independent design. Moreover, recall that despite the fact that the NBC legs are driven by two different PWM signals, a single control signal d is sufficient for creating both converter legs driving PWM signals with corresponding duty cycles d_1 and d_2. Hence, d is treated as the control input and the modulator is assumed to be part of the controlled process.

A. Inner loop controller design and analysis.

The input and output voltages vary very slowly with respect to the inductor current since the bandwidth (BW) of inner controller is much higher than the outer controller BW they may be considered constant when designing the current controller. Inductor current dynamics of the NBC are then given by

$$L\frac{di_L}{dt}=\begin{cases}K_H V_S\cdot d+K_H V_S-V_O-i_L r_{L-Q}, & buck\\ \left(K_H V_S+K_L V_O\right)\cdot d+K_H V_S-K_L V_O-i_L r_{L-Q}, & buck-boost,\\ K_L V_O\cdot d+V_S-K_L V_O-i_L r_{L-Q}, & boost,\end{cases} \quad (8)$$

demonstrating piecewise linear yet operating mode dependent behavior. Taking the Laplace transform of and rearranging results in

$$I_L(s)=\frac{1}{Ls+r_{L-Q}}\left(G_I D(s)+U(s)\right), \quad (9)$$

with

$$G_I=\begin{cases}G_{Ibuck}=K_H V_S, & buck\\ G_{Ibuck-boost}=K_H V_S+K_L V_O, & buck-boost\\ G_{Iboost}=K_L V_O, & boost\end{cases} \quad (10)$$

and

$$U(s)=\begin{cases}K_H V_S-V_O, & buck\\ K_H V_S-K_L V_O, & buck-boost\\ V_S-K_L V_O, & boost\end{cases} \quad (11)$$

denoting control gain and disturbance, respectively, and $D(s)$ symbolizing the Laplace transform of the control signal $d(t)$. A PI controller is selected to compensate the current loop as follows. Defining the nominal control gain as

$$G_{IN} = \frac{1}{3}\left(G_{Ibuck} + G_{Ibuckboost} + G_{Iboost}\right), \tag{12}$$

Eq. (9) may be rearranged as

$$I_L(s) = \frac{1}{Ls + r_{L-Q}}\left(G_{IN}D(s) + U'(s)\right), \tag{13}$$

where

$$U'(s) = \left(Ls + r_{L-Q}\right)U(s) + (G_I - G_{IN})D(s). \tag{14}$$

Consequently, the control-to-output transfer function is given by

$$P_I(s) = \frac{I_L}{D}(s)\bigg|_{U'(s)=0} = \frac{G_{IN}}{L}\left(s + \frac{r_{L-Q}}{L}\right)^{-1} \tag{15}$$

Hence, the transition between modes is equivalent from the control point of view to a step change in disturbance and would be properly rejected by a PI [33] or type-II [34] control structure. Selecting the PI controller

$$C_I(s) = \frac{L}{G_{IN}}\left[\left(2\xi_{Id}\omega_{Id} - \frac{r_{L-Q}}{L}\right) + \omega_{Id}^2\,\frac{1}{s}\right] \tag{16}$$

leads to the nominal closed loop system of the form

$$\frac{I_L}{I_L^{REF}}(s) = \frac{2\xi_{Id}\omega_{Id}s + \omega_{Id}^2}{s^2 + 2\xi_{Id}\omega_{Id}s + \omega_{Id}^2} \tag{17}$$

with ξ_{Id} and ω_{Id} denoting the desired closed loop damping and natural frequency. Furthermore, adding the following pre-filter

$$F(s) = \frac{\omega_{Id}^2}{2\xi_{Id}\omega_{Id}s + \omega_{Id}^2} \tag{18}$$

on the reference signal would bring the nominal closed loop system to the standard second order form of

$$\frac{I_L}{I_{REF}}(s) = \frac{\omega_{Id}^2}{s^2 + 2\xi_{Id}\omega_{Id}s + \omega_{Id}^2}. \quad (19)$$

Nevertheless, actual control gain is G, given by (10) rather than G_N. Consequently, actual closed loop system would be given by

$$\frac{I_L}{I_{REF}}(s) = \frac{2\frac{G_I}{G_{IN}}\xi_{Id}\omega_{Id}s + \frac{G_I}{G_{IN}}\omega_{Id}^2}{s^2 + 2\frac{G_I}{G_{IN}}\xi_{Id}\omega_{Id}s + \frac{G_I}{G_{IN}}\omega_{Id}^2} \quad (20)$$

in case without the pre-filter and

$$\frac{I_L}{I_{REF}}(s) = \frac{\frac{G_I}{G_{IN}}\omega_{Id}^2}{s^2 + 2\frac{G_I}{G_{IN}}\xi_{Id}\omega_{Id}s + \frac{G_I}{G_{IN}}\omega_{Id}^2} \quad (21)$$

with the use of pre-filter (18). It may then be concluded that while the system remains stable with unity DC gain, the closed loop natural frequency and damping vary according to NBC operating point and operation mode as

$$\omega_I = \sqrt{\frac{G_I}{G_{IN}}}\omega_{Id}, \quad \xi_I = \sqrt{\frac{G_I}{G_{IN}}}\xi_{Id}. \quad (22)$$

The disturbance rejection is given by

$$\frac{I_L}{U}(s) = \frac{1}{L}\frac{s}{s^2 + 2\frac{G_I}{G_{IN}}\xi_{Id}\omega_{Id}s + \frac{G_I}{G_{IN}}\omega_{Id}^2} = \frac{1}{L}\frac{s}{s^2 + 2\xi_I\omega_I s + \omega_I^2}, \quad (23)$$

i.e. zero steady state error at DC is preserved at all times despite the natural frequency and damping variations.

B. Outer loop controller design and analysis.

In cascade control construction, the inner loop is decoupled from the outer loop at least by one order of magnitude in frequency domain, inductor current may be assumed to track its reference perfectly as $i_L(t) \approx i_L^{REF}(t) \ \forall t$ for some slowly time–varying reference. This assumption was made in e.g. [31]. Consequently, inductor current reference serves as the power loop control input. NBC output capacitor dynamics is then given by

$$C_2 \frac{dv_O}{dt} = \begin{cases} i_{REF} + \dfrac{V_{BUS2} - v_O}{r_{BUS2}} - \dfrac{p_L}{v_O}, & buck \\ K_L(1-d) i_{REF} + \dfrac{V_{BUS2} - v_O}{r_{BUS2}} - \dfrac{p_L}{v_O}, & boost \,\&\, buck-boost \end{cases} . \quad (24)$$

Furthermore, the NBC output power may be obtained from (5b). Hence, the output power dynamics is nonlinear, calling for a linearization procedure. Splitting the time-based variables into DC and AC components,

$$i_{REF} = I_{REF} + \tilde{i}_{REF}, v_O = V_O + \tilde{v}_O, d = D + \tilde{d}, p_L = P_L + \tilde{p}_L, p_O = P_O + \tilde{p}_O \quad (25)$$

and substituting into (24) and (5b) results in the following inductor current reference toNBC output power small-signal transfer functions,

$$\tilde{P}_p(s) = \frac{\tilde{p}_O}{\tilde{i}_{REF}}(s) = \\ = \begin{cases} \left(\dfrac{V_O(2V_O - V_{BUS2})}{2V_O - (V_{BUS2} + I_{REF} r_{BUS2})} \right) \dfrac{1}{1 + \left(\dfrac{C_2 V_O r_{BUS2}}{2V_O - (V_{BUS2} + I_{REF} r_{BUS2})} \right) s}, & buck \\ \left(\dfrac{K_L(1-D) V_O(2V_O - V_{BUS2})}{2V_O - (V_{BUS2} + K_L(1-D) I_{REF} r_{BUS2})} \right) \dfrac{1}{1 + \left(\dfrac{C_2 V_O r_{BUS2}}{2V_O - (V_{BUS2} + K_L(1-D) I_{REF} r_{BUS2})} \right) s}, & boost \,\&\, buck-boost \end{cases} \quad (26)$$

linearized around the operating point given by

$$I_{REF}=\begin{cases}\dfrac{P_O}{V_O}, & buck\\ \dfrac{P_O}{K_L(1-D)V_O}, & boost\ \&\ buck-boost\end{cases}. \tag{27}$$
$$V_O^2-V_{BUS2}V_O+r_{BUS2}\left(P_L-P_O\right)=0,\quad P_O=P_{REF}$$

Note that since the values of V_{BUS2} and V_O are close, differing only by the r_{BUS2} voltage drop, the obtained transfer functions are stable and the plant may be rearranged into the following general form,

$$\tilde{P}_p(s)=\frac{G_P}{1+\tau s} \tag{28}$$

with

$$G_P=\begin{cases}G_{Pbuck}=\dfrac{V_O\left(2V_O-V_{BUS2}\right)}{2V_O-\left(V_{BUS2}+I_{REF}r_{BUS2}\right)}, & buck\\ G_{Pbuck-boost}=\dfrac{K_L(1-D)V_O\left(2V_O-V_{BUS2}\right)}{2V_O-\left(V_{BUS2}+K_L(1-D)I_{REF}r_{BUS2}\right)}, & buck-boost\\ G_{Pboost}=\dfrac{K_L(1-D)V_O\left(2V_O-V_{BUS2}\right)}{2V_O-\left(V_{BUS2}+K_L(1-D)I_{REF}r_{BUS2}\right)}, & boost\end{cases} \tag{29}$$

and

$$\tau=\begin{cases}\tau_{buck}=\dfrac{C_2V_Or_{BUS2}}{2V_O-\left(V_{BUS2}+I_{REF}r_{BUS2}\right)}, & buck\\ \tau_{buck-boost}=\dfrac{C_2V_Or_{BUS2}}{2V_O-\left(V_{BUS2}+K_L(1-D)I_{REF}r_{BUS2}\right)}, & buck-boost\\ \tau_{boost}=\dfrac{C_2V_Or_{BUS2}}{2V_O-\left(V_{BUS2}+K_L(1-D)I_{REF}r_{BUS2}\right)}, & boost\end{cases}. \tag{30}$$

It must be emphasized that the value of D is different in buck-boost and boost modes, therefore the plants are non-similar as well even though the general representations are alike. A PI controller is selected to compensate the power loop as follows. Defining the nominal plant gain and time constant as

$$G_{PN}=\frac{1}{3}\left(G_{Pbuck}+G_{Pbuckboost}+G_{Pboost}\right) \tag{31}$$

$$\tau_N = \frac{1}{3}\left(\tau_{buck} + \tau_{buckboost} + \tau_{boost}\right), \tag{32}$$

respectively, the nominal plant is given by

$$\tilde{P}_{pN}(s) = \frac{G_{PN}}{1+\tau_N s}. \tag{33}$$

Selecting the PI controller

$$C_P(s) = \frac{\omega_{Pd}}{G_{PN}} \frac{1+\tau_N s}{s} \tag{34}$$

leads to the nominal closed loop system of the form

$$\frac{\tilde{p}_O}{\tilde{p}_{ref}}(s) = \frac{\omega_{Pd}}{s+\omega_{Pd}} \tag{35}$$

with ω_{Pd} denoting the desired closed loop bandwidth. Nevertheless, actual plant is (28) rather than (33). Consequently, actual closed loop system would be given by

$$\frac{\tilde{p}_O}{\tilde{p}_{ref}}(s) = \frac{\frac{G_P}{G_{PN}}\omega_{Pd}\left(1+\tau_N s\right)}{\tau s^2 + \left(1+\frac{G_P}{G_{PN}}\omega_{Pd}\tau_N\right)s + \frac{G_P}{G_{PN}}\omega_{Pd}}. \tag{36}$$

It may then be concluded that while the system remains stable with unity DC gain,the first-order behavior is no longer maintained (the resulting system possesses two poles and one stable zero).

The disturbance rejection is given by

$$\frac{\tilde{P}_p(s)}{1+C_P(s)\tilde{P}_p(s)}(s) = \frac{s}{\tau s^2 + \left(1+\frac{G_P}{G_{PN}}\omega_{Pd}\tau_N\right)s + \frac{G_P}{G_{PN}}\omega_{Pd}} \tag{37}$$

i.e. zero steady state error at DC is preserved at all times despite the parameters variations.

IV. DESIGN EXAMPLE

Consider a topology of Fig. 1with relevant system parameters summarized in Table I.

TABLE I

System Data

Parameter	Value	Units
FC voltage (v_S) range	24 – 46	V
Battery voltage (v_O) range	21 – 29.4	V
Battery resistance (R_{BAT}) range	20 – 40	mΩ
NBC output power (p_O) range	0 – 200	W
NBC input capacitance (C_1)	470	µF
NBC inductance (L)	10	µH
NBC output capacitance (C_2)	470	µF
NBC modulator limits ($-V_L = V_H$)	0.05	---
NBC switching frequency (T^{-1})	100	kHz

According to (3) and (4), operation mode of the NBC and the corresponding steady-state value of the control signal $d$may then be determined from

$$Operating\ Mode = \begin{cases} buck, & \frac{V_O}{V_S} < 0.9 \\ buck-boost, & 0.9 < \frac{V_O}{V_S} < 1.1 \\ boost, & \frac{V_O}{V_S} > 1.1 \end{cases} \quad (38)$$

and

$$D=\begin{cases}1.05\dfrac{V_O}{V_S}-1, & buck\\ \left(\dfrac{V_O}{V_S}-1\right)\left(\dfrac{V_O}{V_S}+1\right)^{-1}, & buck-boost\\ 1-1.05^{-1}\dfrac{V_S}{V_O}, & boost,\end{cases} \tag{39}$$

respectively.

A. Current loop design.

The family of all the possible current loop plants is shown in Fig. 6. The nominal plant is obtained by selecting nominal FC and battery values as 34 V and 25.9 V, respectively.

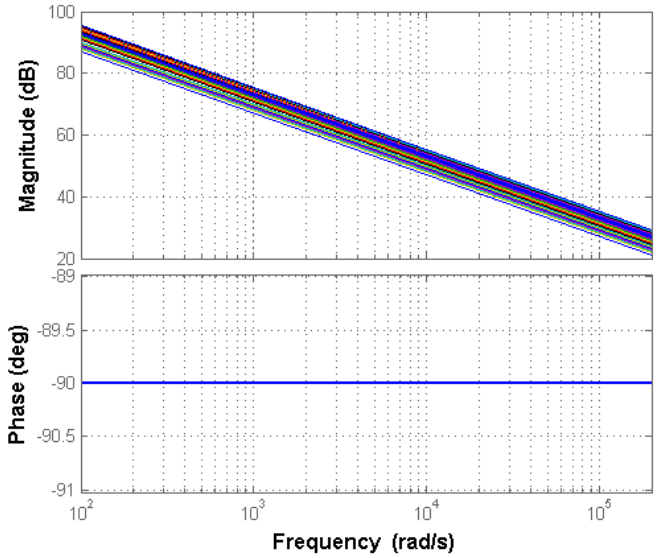

Fig. 6. Family of current loop plants.

The current loop controller is then designed according to (16) with ξ_{Id} = 1 and ω_{Id} = 20000 rad/s without a pre-filter. The resulting current loop gains family is depicted in Fig. 7, verifying stability at all operating points according to resulting phase margin (PM) range. Corresponding closed loop tracking and disturbance rejection capabilities are given in Figs. 8 and 9, respectively, further enforcing the outcomes of the analysis above.

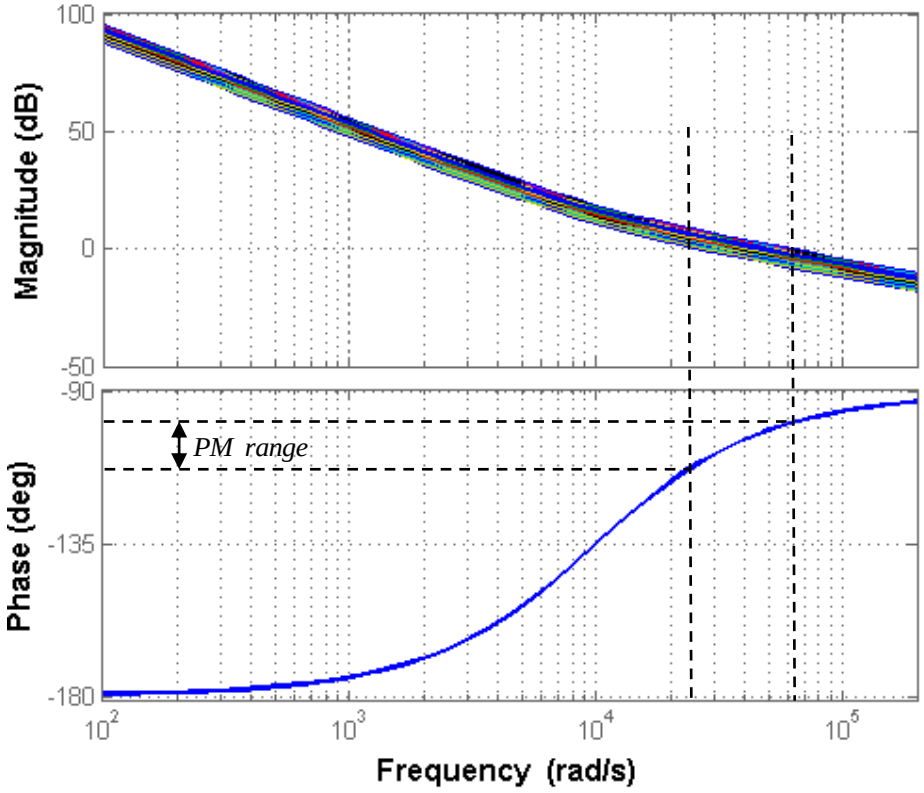

Fig. 7. Family of current loop gains.

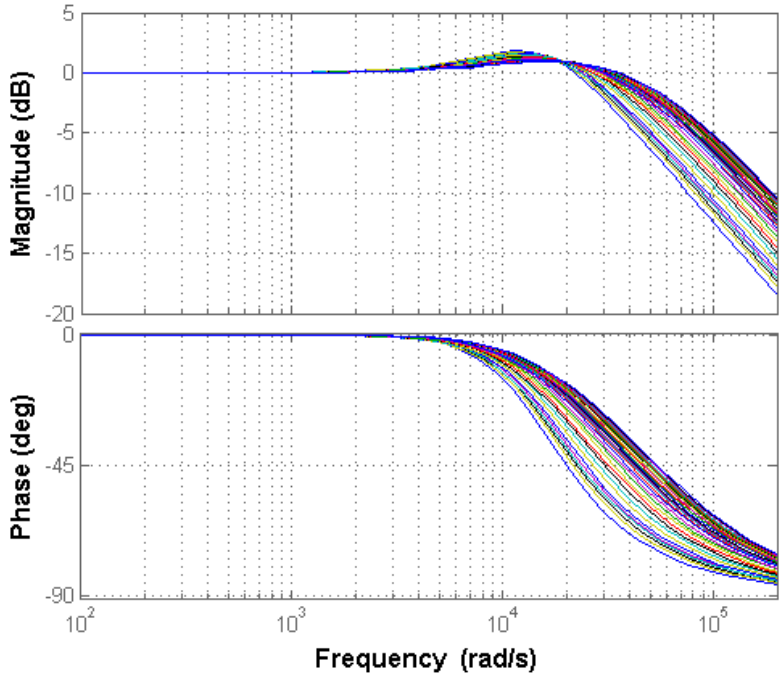

Fig. 8. Inductor current tracking behavior throughout the operating range.

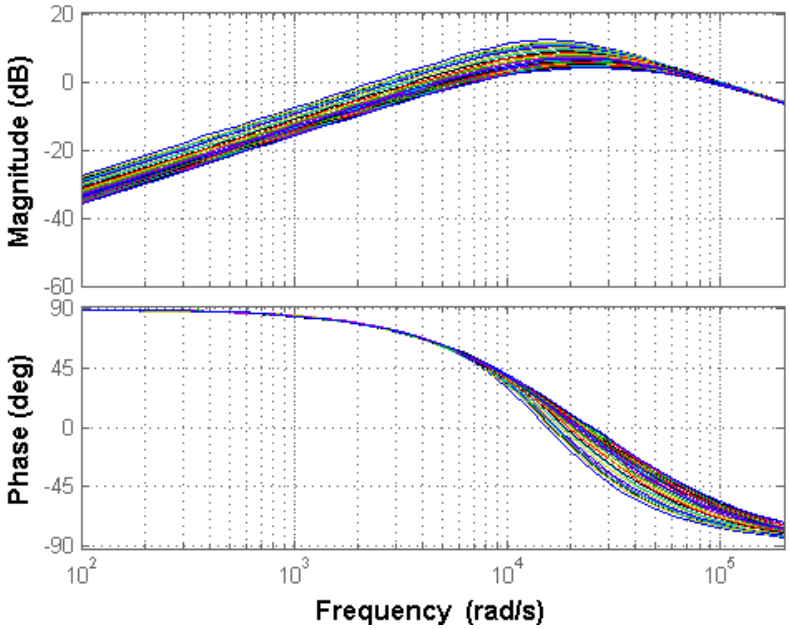

Fig. 9. Current loop disturbance rejection capabilities throughout the operating range.

B. Power loop design.

The family of all the possible power loop plants is shown in Fig. 10, where the nominal plant is obtained by selecting nominal FC and battery voltage as 34V and 25.9V respectively, and assuming nominal NBC and load power as 200W and 250 W, respectively.

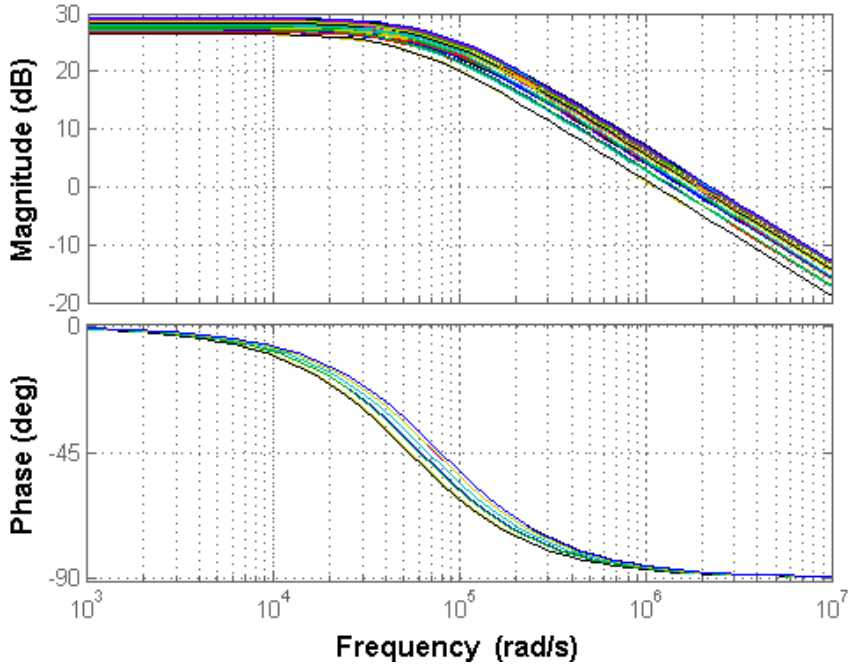

Fig. 10. Family of power loop plants.

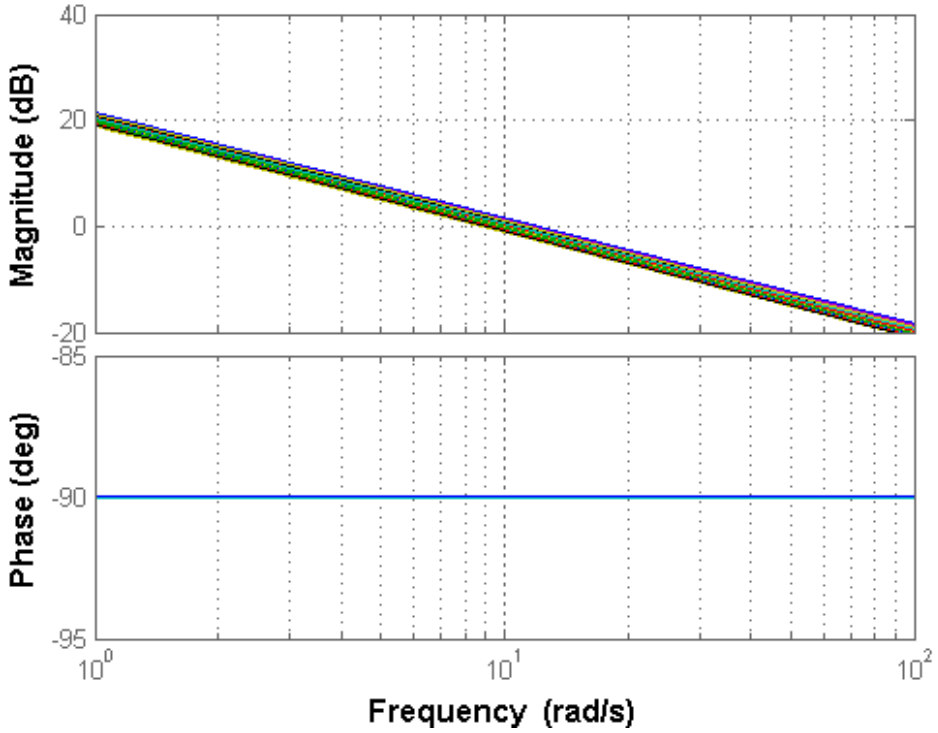

Fig. 11. Family of power loop gains.

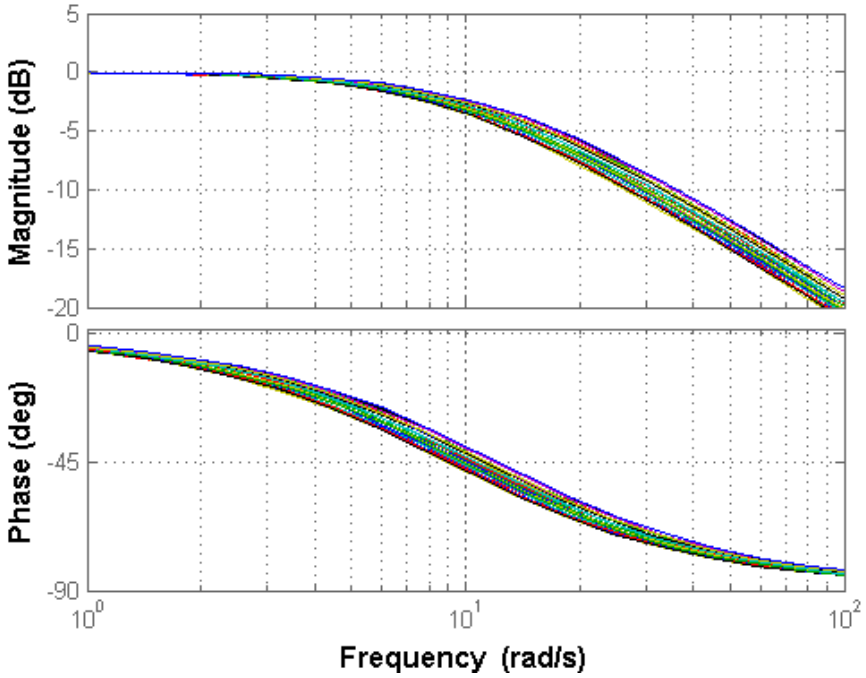

Fig. 12. NBC output power tracking behavior throughout the operating range.

The power loop controller is then designed according to (34) with ω_{Pd} = 10 rad/s (note the validity of loop decoupling assumption). The resulting power loop gains family is illustrated

in Fig. 11, confirming stability at all operating points. Corresponding closed loop tracking and disturbance rejection abilities of the system are given in Figs. 12 and 13, respectively, validating the analysis conclusions.

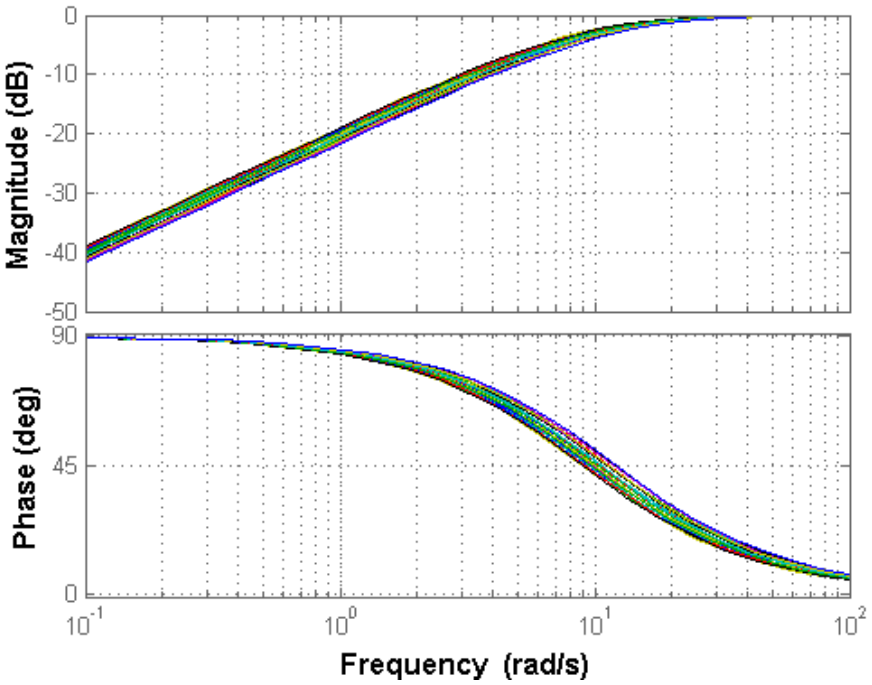

Fig. 13. Power loop disturbance rejection capabilities throughout the operating range.

C. Time domain simulations.

PSIM software-based time-domain simulations were carried out in order to verify the operation of the proposed control structure. Li-Po battery and PEM FC models were developed based on the data, experimentally extracted by dischargingа 7-cell, 4.4 Ah ThunderPower Li-Po battery and a 200W H-200 Horizon Proton Exchange Membrane (PEM) FC (utilized in the experimental prototype, as shown below at different rates. Lossless NBC was assumed in the simulations and the load was represented by a controlled power sink.

In the first two simulations, tracking capabilities of the system were examined as follows. The load was disconnected and the range extender was operated to charge the battery in a

step-like manner by appropriately increasing (the first simulation) and decreasing (the second simulation) the power reference signal. The results are shown in Figs. 14 and 15, demonstrating excellent tracking capabilities of the system.

In the last simulation, disturbance rejection capabilities of the system were tested. The NBC output power reference was set to 200W and the load power was varied in a step-like manner. The results are shown in Fig. 16., validating zero steady-state error operation, as predicted.

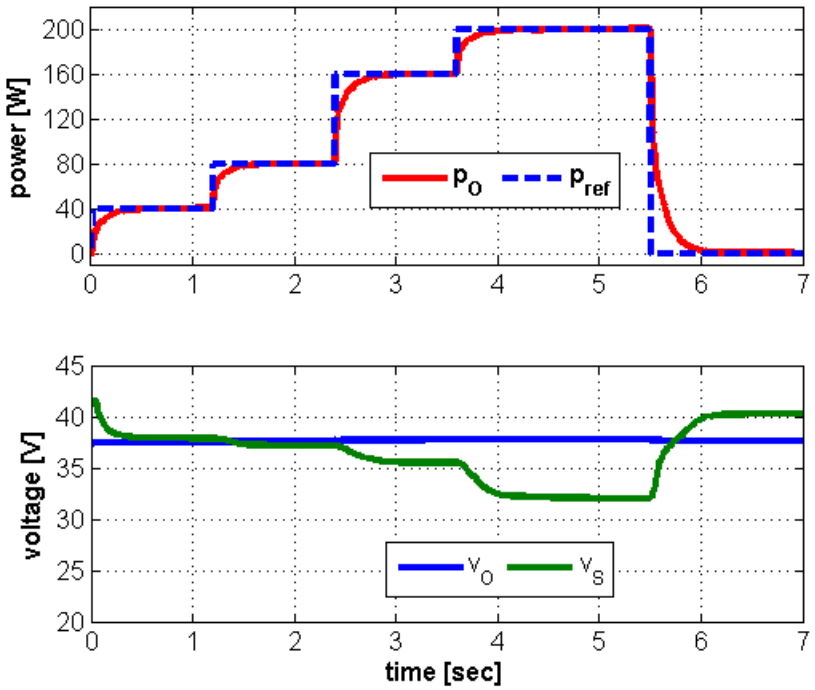

Fig. 14. Simulation results, step-up power tracking performance: top – reference and measured NBC output power; bottom – input and output NBC voltages.

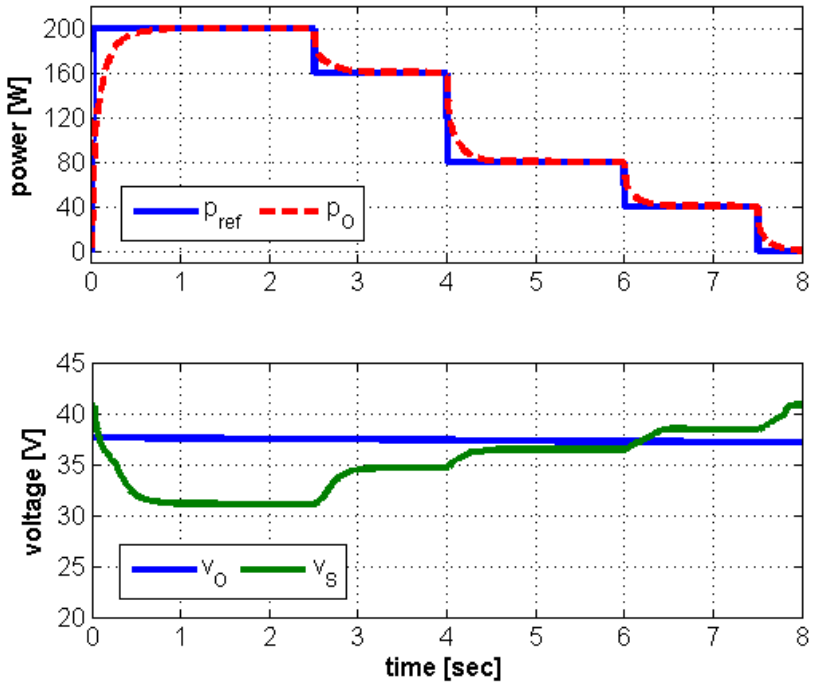

Fig. 15. Simulation results, step-down tracking performance: top – reference and measured NBC output power; bottom – input and output NBC voltages.

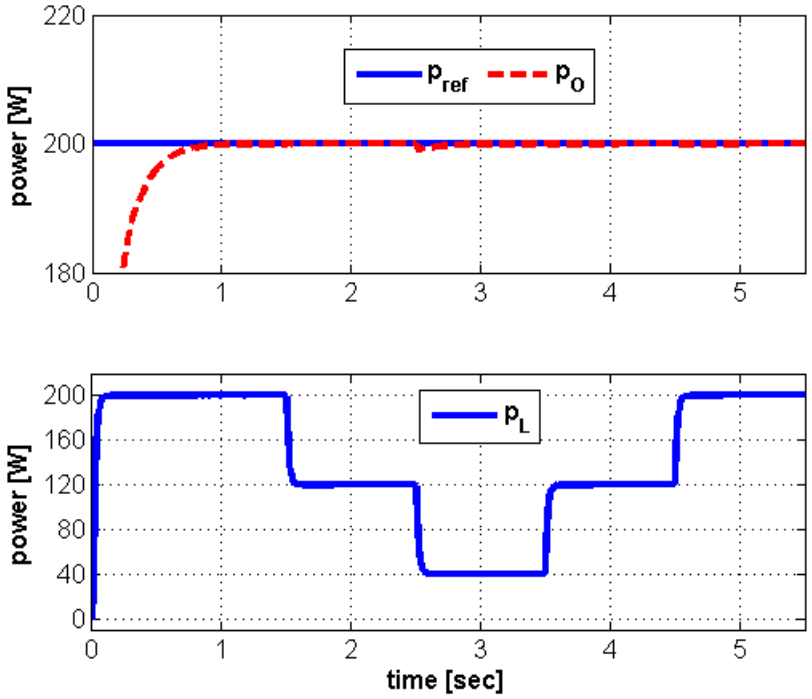

Fig. 16. Simulation results, disturbance rejection performance: top – reference and measured NBC output power; bottom – load power.

V. EXPERIMENTAL VALIDATION

In order to experimentally validate the design example, an experimental prototype was built and tested. Experimental setup is pictured in Fig. 17. An analog PI controller was utilized as current loop compensator while the power controller was realized digitally using a TMS320F28335 Texas Instruments digital signal processor (DSP). A real aerial vehicle propulsion unit (Sensorless DC/AC converter based driver + Permanent Magnet Synchronous Motor + Propeller) was utilized as the power load. Please note, the objectives of this work in the NBC and its regulator (implemented with DSP).

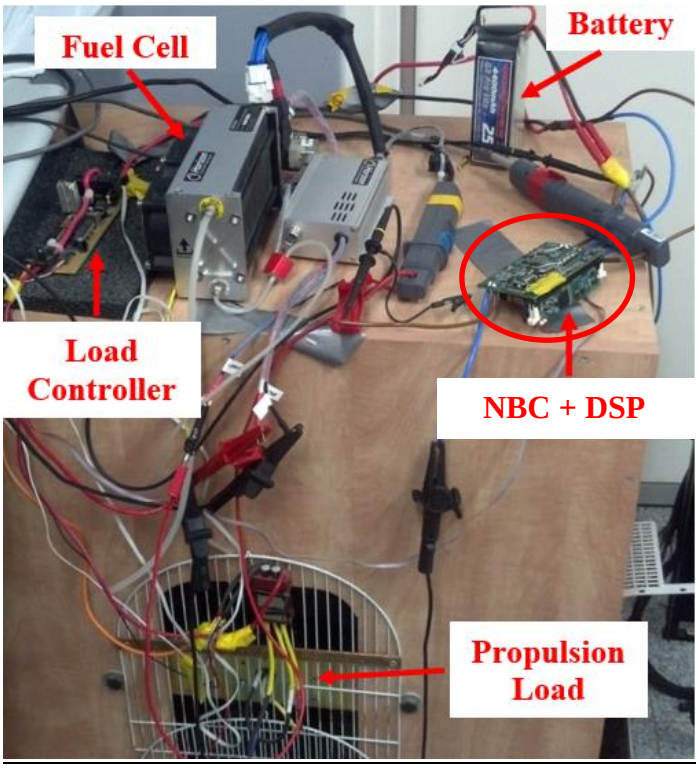

Fig. 17. Experimental setup.

In order to gain control over the input power of propulsion system, a dedicated load controller was designed, operating as follows. The desired load power $p_{L,ref}$ is set by the user and transferred to the load controller from a PC via the UART interface (please note, that

$p_{L,ref}$ is same as for the NBC power reference). In addition, load voltage and current are transferred to the controller as well in order to evaluate the instantaneous load lower. The load controller processes the difference between the desired and instantaneous load powers and sends an appropriate throttle command to the propulsion unit driver, as shown in Fig. 18.

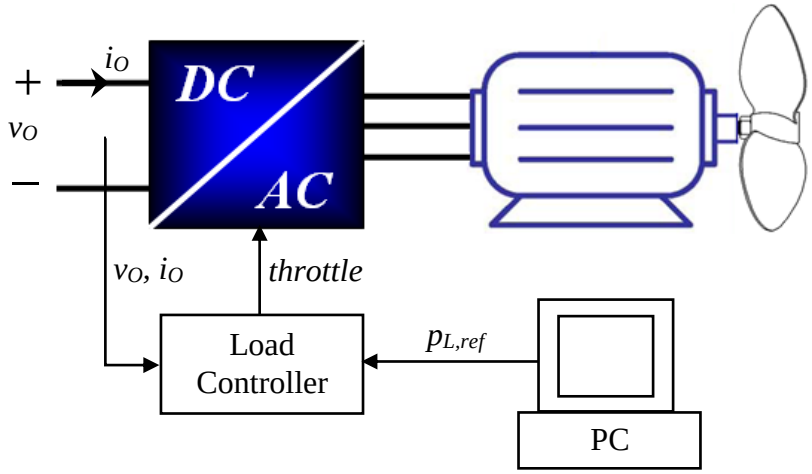

Fig. 18. Power load realization.

Experimental data was acquired using a 400 MHz Lecroy Wave Runner 44 XI-A oscilloscope and two AP015 Lecroy current probes. Three experiments were carried out in accordance with the above-demonstrated simulations. Tracking capabilities of the system are shown in Figs. 19 and 20, while disturbance rejection is demonstrated in Fig. 21 (load power reference is shown as well to verify load controller operation). All the experiments closely resemble simulation results, validating the proposed approach.

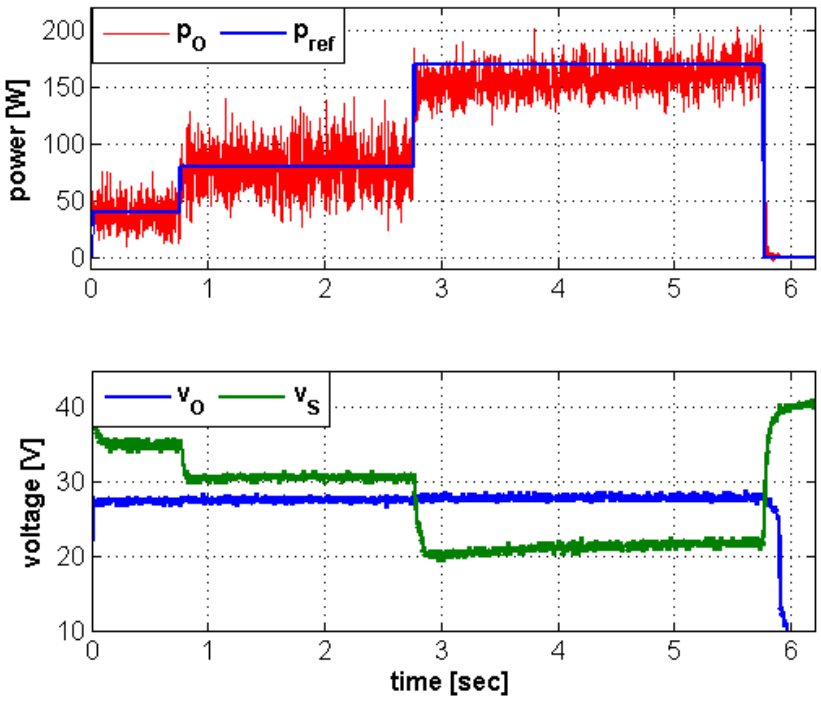

Fig. 19. Experimental results, step-up power tracking performance: top – reference and measured NBC output power; bottom – input and output NBC voltages.

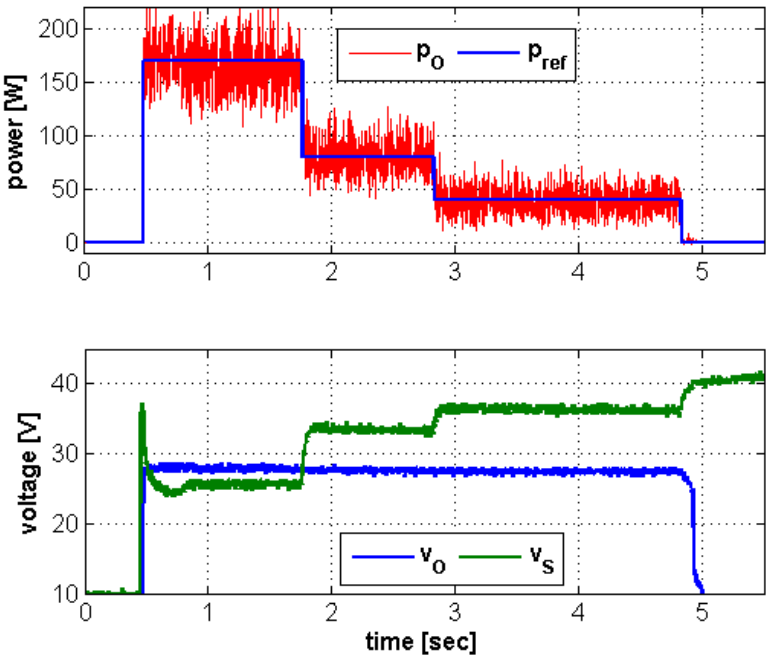

Fig. 20. Experimental results, step-down tracking performance: top – reference and measured NBC output power; bottom – input and output NBC voltages.

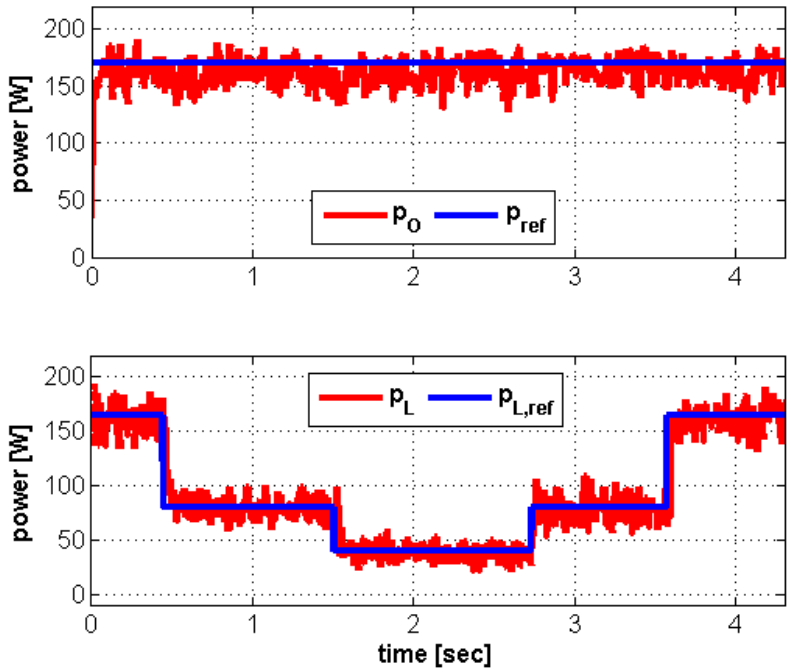

Fig. 21. Experimental results, disturbance rejection performance: top – reference and measured NBC output power; bottom – reference and measured load input power.

VI. CONCLUSIONS

A cascaded output power control structure for a non-inverting buck-boost converter governed by a recently proposed dual carrier modulator was derived in this paper based on appropriate small-signal modeling. The control structure allows precise power tracking and decent disturbance rejection during converter mode transitions and load power variations. In order to verify the proposed design, an experimental setup was built and tested. Close resemblance of simulation and experimental results enforced the feasibility of the suggested principle and control structure.

REFERENCES

[1] Aharon I, Kuperman A. Topological overview of powertrains for battery powered vehicles with range extenders. *IEEE Trans. Power Electronics*. 2011;26:868–76.

[2] Levron Y, Shmilovitz D. Optimal power management in fueled systems with finite storage capacity. IEEE Trans. Circuits Syst. I Aug. 2010;57(8):2221-31.

[3] Chen Y.H, Chen C.Y, Lee S.C. Technology forecasting and patent strategy of hydrogen energy and fuel cell technologies. J. Hydrogen Energy June. 2011;36(12):6957–69.

[4] Sakamoto Y, Hoshi N, Murooka S, Meifen C, Yoshizaki A, Hirata K. Basic study on fuel-cell-hybrid-electric-vehicle fueled by sodium borohydride. In: Proc. IPEC June. 2011; p. 814–9.

[5] Gadelovits S, Kuperman A, Sitbon M, Aharon I, Singer S. Interfacing Renewable Energy Sources for Maximum Power Transfer - Part I: Statics. Renew. Sust. Energy Reviews 2014;31:501–508.

[6] Microgrid Exchange Group. (2011, Aug). DOE Microgrid Workshop Report [Online]. Available: http://energy.gov/oe/downloads/mocrogrid-workshop-report-august-2011

[7] Carpinelli G, Mottola F, Proto D and Varilone P. Minimizing Unbalances in Low-Voltage Microgrids: Optimal Scheduling of Distributed Resources. J. Applied Energy Apr. 2017;191:170–82.

[8] Y. J. L. A. K. A. C. Ali Emadi. Digital Combination of Buck and Boost Converters to Control a Positive Buck–Boost Converter and Improve the Output Transients. IEEE TRANSACTIONS ON POWER ELECTRONICS. 2009;24(5):1267-79.

[9] Lee Y.J,.Khaligh A, Emadi A. A Compensation Technique for Smooth Transitions in a Noninverting Buck–Boost Converter. IEEE Transactions on Power Electronics2009;24:1002-16.

[10] Kuperman A, Aharon I, Malki S, Kara A., Design of a Semiactive Battery-Ultracapacitor Hybrid Energy Source. IEEE Transactions on Power Electronics2013; 28:806-15.

[11] Badawy M.O, Sonior Y, De Abreu-Garcia J.A. A Novel Control for a Cascaded Buck–Boost PFC Converter Operating in Discontinuous Capacitor Voltage Mode.IEEE Trans. Industrial Electronics2016;63(7):4198-210.

[12] H. Xiao and S. Xie. Interleaving double-switch buck-boost converter. IET Power Electronics July 2012;5(6):899-908,

[13] Ishaque K. Salam Z. and George L. The performance of perturb and observe and incremental conductance maximum power point tracking method under dynamic weather conditions. J. Applied Energy. Apr. 2014;119:228-36.

[14] Durán E,AndújarJ.M, Segura F and BarragánA.J.A.High-Flexibility DC Load for Fuel Cell and Solar Arrays Power Sources Basedon DC-DC Converter. J. Applied Energy Jan. 2011;88(5):1690-702.

[15] Teresa D, Antonio F, Luigi S, Alessandro A, and Marco F. A New Approach to Calculating Endurance in Electric Flight and Comparing Fuel Cells and Batteries.J. Applied Energy Feb. 2017;187:807–17.

[16] Schaltz E. Rasmussan P.O. and Khaligh A. Non-Inverting Buck-Boost Converter for Fuel Cell application. in Proc. 34th Annual Conference of the IEEE Industrial Electronics Society (IECON). 2008.

[17] Liao H. K. Liang T. J. Yang L. S. and Chen J. F. Non-inverting buck–boost converter with interleaved technique for fuel-cell system. IET Power Electronics. 2012;5(8): 1379-88.Aharon I. Shmilovitz D. and Kuperman A. Robust UDE Controller for Energy Storage Application. IEEE ICRERA 2015:1-6.

[18] Huang P.C, Wu W.Q, Ho H.H,Chen K.H.Hybrid Buck–Boost Feed-Forward and Reduced Average Inductor Current Techniques in Fast Line Transient and High-Efficiency Buck–Boost Converter. IEEE Trans. Power Electronics2011;26(3):868–76.
[19] Laura T, Raffaello C, Daniele C, and Paolo I. Energy Management of A Plug-In Fuel Cell/Battery Hybrid Vehicle With On-Board Fuel Processing.J. Applied Energy Dec. 2016;184:140–54.
[20] Junqiu L, Xin J, and Rui X. Multi-Objective Optimization Study of Energy Management Strategy and Economic Analysis for A Range-Extended Electric Bus. J. Applied EnergyNov. 2016;xxx(xx):1–10.
[21] Ziyou S, Jianqiu L, Xuebing H, Liangfei X, Languang L, Minggao O, and Heath H. Multi-Objective Optimization of ASemi-Active Battery/Supercapacitor Energy Storage System for Electric Vehicles.J. Applied Energy Dec. 2014;135:212–24.
[22] Paul C, Scott C, Shean H, Lonnie L, Brian P, Robert W, Roderick J, and Johney G.J. Development of A Range-Extended Electric Vehicle Pwertrain for An Integrated Energy Systems Research Printed Utility Vehicle.J. Applied Energy Apr. 2017;191:99–110.
[23] Junqiu L, Yihe W, Jianwen C, and Xiaopeng Z. Study on Energy Management Strategy and Dynamic Modeling for Auxiliary Power Units in Range-Extended Electric Vehicles.J. Applied Energy Sept. 2016;xxx:1–13.
[24] Waffler S,Kolar J. A Novel Low-Loss Modulation Strategy for High-Power Bidirectional Buck + Boost converters. IEEE Transactions on Power Electronics June. 2009;24(6):1589-99.
[25] Rodriguez M, Stahl G, Corradini L,Maksimovic D.Smart DC Power Management System Based on Software-Configurable Power Modules.IEEE Trans. Power ElectronicsApr. 2013;28(4):1571-86.
[26] Badawy M.O, Sonior Y, De Abreu-Garcia J.A.A Novel Control for ACascaded Buck–Boost PFC Converter Operating in Discontinuous Capacitor Voltage Mode. IEEE Trans. Industrial Electronics2016;63(7):4198-210.
[27] Aharon I, Kuperman A,Shmilovitz D. Analysis of Dual-Carrier Modulator for Bidirectional Non-Inverting Buck-Boost Converter.IEEE Trans. Power ElectronicsFeb. 2015;30(2):840-8.
[28] Erickson R.W, Maksimovic D. Fundamentals of Power Electronics. Second Edition.Kluwer Academic;January 2001.
[29] Seok-Kyoon K, and kyo-Beum L. Robust Feedback-Linearizing Output VoltageRegulator for DC/DC Boost Converter. IEEE Trans. Industrial Electronics Nov. 2015;62(11):7127–35.
[30] Wei C.L, Chen C.H, u K.C,, Ko I.T. Design of An Average-Current-Mode Noninverting Buck-Boost DC-DC Converter With Reduced Switching and Conduction Losses. IEEE Transactions on Power ElectronicsDec. 2012;27(12):4934–43.
[31] Jones D.C,Erickson R.W. Buck-Boost Converter Efficiency Maximization Via A Nonlinear Digital Control Mapping for Adaptive Effective Switching Frequency. IEEE Journal of Emerging and Selected Topics in Power Electronics Sept. 2013;1(3):153–65.
[32] Chen Z.Double Loop Control of Buck-Boost Converters for Wide Range of Load Resistance and Reference Voltage. IETControl Theory and Appl 2012: 6(7):900–10.
[33] Zhifu W, Yupu W, and Yinan R. Design of Closed-Loop Control System for ABidirectional Full Bridge DC/DC Converter. J. Applied Energy Dec. 2016;xxx:1–9.
[34] Ghosh A, Banerjee S, Sarkar M.K, Dutta P.Design and Implementation of Type-II and Type-III Controller for DC–DC Switched-Mode Boost Converter By Using K-Factor Approach and Optimization Techniques. IET Power Electronics 2015;9(5):938-50.